Simulating Liquid Crystals

Kit Gallagher *Supervisors: Prof Erika Eiser, Mr Jiaming Yu*

May 16, 2021

The specificity of DNA base-pair interactions gives considerable functional control in the design of anisotropic nano-particles, enabling the formation of a range of liquid crystal phases. Initial benchmarked tests confine the critical volume fraction of the nematic phase transition for linear ds-DNA mesogens to within 5% of the theoretical value over a range of aspect ratios. I then introduce a novel 'nunchuck' mesogen – two rigid rods of ds-DNA connected via a flexible linker of ss-DNA, and demonstrate the existence of an entropy-driven phase transition to a quasi-nematic (S = 0.58) phase in this system. I outline further evidence for the existence of more exotic 'herringbone', twisted-nematic and biaxial-nematic phases through the use of the pair-wise orientational correlation function. Finally, I present an alternative method for phase identification through the study of dynamic properties, and identify the formation of nematic and smectic phases through the measurement of directional diffusion coefficients.

Supplementary Material: *If necessary*
Online Lab-book: *To be included*

Contents

1 Introduction

Since Kirkwood's prediction of an ~~entropy-driven~~ entropically driven ordering transition in the freezing of hard spheres [**Kirkwood1954**], ~~entropy-driven~~ entropically driven phase transitions have been the subject of much attention [**Kerr1993**, **Frenkel1999**]. Their relevance to colloidal systems is often underestimated, but gives rise to a range of diverse phase behaviour [**Adams1998**, **Anderson2002**, **Forsyth1978**]. In particular, there is a wealth of (primarily experimental) studies of 'bent-core' liquid crystals — rigid rods with a central bend [**Takezoe2006**, **Etxebarria2008**, **Yang2018**].

These molecules have primarily been used for their polarity however; here we consider a bent-core system with no polarity, ~~which displays true entropy-driven~~ which displays true entropically driven phase transitions. We conduct molecular dynamics simulations on a course-grained model to study such transitions in a system of 'nunchucks', molecules consisting of two rigid rods of double stranded (ds-) DNA, connected via a flexible linker of single stranded (ss-) DNA. This linker allows the configuration to vary from fully stretched to folded.

DNA is chosen due to ~~availability through polymerase chain reactions, its exact design in terms of sequence and thus its~~ its availablity through PCR, its exact design in terms of sequence and thus its reproducibly on the nanoscale. The techniques in phase simulation developed here are relevant to more complex DNA structures, such as in the development of liquid crystal behaviour in DNA origami [**Cha2015**, **Wang2018**], or in ~~entropy-driven~~ entropy driven nano-structure self-assembly [**Barry2010**, **Lin2000**].

In Section 2 ~~I outline the thermodynamic~~ I outline the thermodynamic theory behind liquid crystals and phase transitions, before describing the previous experimental and simulation work in this area. Section 3 details the computational approach taken, in both simulation and analysis, ~~and outlines~~ and outlines the coarse-grained model used. ~~I~~ We then benchmark the techniques used against known results for a system of rigid rods in Section 4, outlining simulations from both dilute and crystalline initial configurations (with subsequent contraction or expansion respectively). These approaches are then applied to the nunchuck system in Section 5, with two separate coarse-grained representations of the central bend in the nunchuck molecules (fixed angle or fixed bond rigidity). Finally, ~~I~~ we also consider a novel approach to phase characterisation though dynamic properties in Section 6, using the anisotropy of the coordinate diffusion coefficients to identify the onset of order in dynamic simulations.

2 Background

2.1 Liquid Crystals

First identified as an intermediary phase between solids and liquids in 1888 by Friedrich Reinitzer [**Reinitzer1888**], the fundamental classes of liquid crystals were characterised in the following decades by Georges Friedel (among others) [**Friedel1922**]. Research into the applications of liquid crystals only became widespread in the 1960s, however, initiated by the seminal research of George William Gray [**Gray1962**], and culminating Heilmeier's development of the first liquid crystal display [**Heilmeier1969**, **Heilmeier1968**]. Later, in 1991, Pierre-Gilles de Gennes received the Nobel Prize in physics "*for discovering that methods developed for studying order phenomena in simple systems can be generalized to more complex forms of matter, in particular to liquid crystals and polymers*" [**DeGennes1992**].

In the most general sense, liquid crystals are states of matter displaying properties between those of conventional liquids and solid crystals. For this reason, they are also known as mesomorphic phases, with individual molecules being referred to as mesogens, and these terms will be used interchangeably through this report. While solid crystals display long range periodic order in three dimensions (and isotropic liquids in none), liquid crystals have a degree of long range order in some (but not all) spatial dimensions. There are three fundamental classes [**DeGennes1993**], visualised in Figure 1.

- **Nematic:** No positional order, but orientational order as molecules[1] tend to point in the same direction.

- **Smectic:** One dimensional positional order, so has the appearance of 2D liquid layers separated by a well defined spacing.
- **Columnar:** Two dimensional positional order, so has the appearance of an 2D array of liquid tubes.
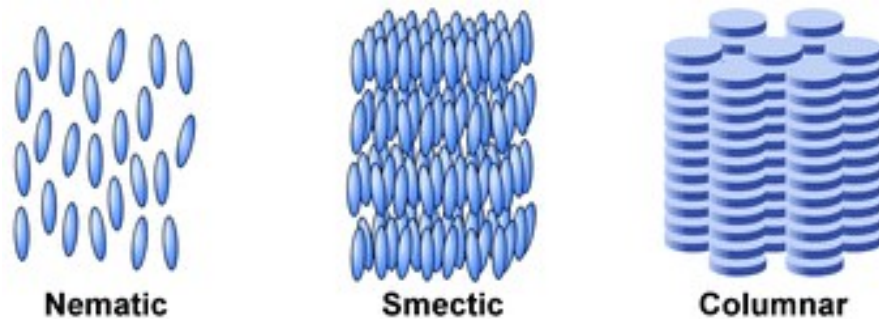
Figure 1: *Representation of the three liquid crystal phase classes, reproduced from Kato et al. [**Kato2007***] with permission. Note the distinct layers in the smectic and columnar phases, and the different class of molecule in the columnar phase.*

It should be noted that the higher order phases (smectic and columnar) also display orientational order throughout the body. This is fundamental to the formation of liquid crystals, and so (almost) all mesogenic molecules are anisotropic. We will see later that the degree of anisotropy affects the stability of different phases.

As is visible in Figure 1, this anisotropy can come in different forms. 'Rod-like' molecules (where anisotropy is in the form of one elongated axis) are the oldest, and most ~~common,~~ common form of liquid crystal. They favour the formation of nematic and smectic phases, and ~~are~~ are the focus of this report. ~~Disk shaped~~ Disk-shaped (discotic) molecules, discovered by Chandrasekhar in 1977 [**Chandrasekhar1977**], have one compressed axis, and favour the formation of other nematic or columnar phases. In 1987, Lam predicted the existence of a sub-class of 'bowlic' molecules which break the up-down symmetry of discotic molecules [**LinLei1988**], which were subsequently found experimentally [**Zimmermann1985**, **Malthete1985**].

Liquid crystals can also be categorised by the driving force behind their transition. ~~Samples only containing one type of smaller molecules undergo thermally-driven phase transitions, and are called thermotropic liquid crystals. By contrast, larger molecules or colloids dispersed in a continuous solvents are classed as lyotropic; their phase transitions are concentration driven [DeGennes1993]. Here I focus lyotropic, entropy-driven phase transitions, where the mesogens (here DNA-nanocolloids) interact purely repulsively. Our studies represent a benchmark for designer-made, DNA-based systems.~~ Samples containing only one type of smaller molecules undergo thermally driven phase transitions, which are call

~~Entropy-driven phase transitions~~ Entropically driven phase-transitions are often seen as counter-intuitive, as such transitions rely on an increase in microscopic disorder from an increase in visible order (an example is given in Section 2.2). Once considered an abnormality, Frenkel famously noted that "*...such phase transformations may not be interesting exceptions, but the rule!*" [**Frenkel1999**].

2.2 Onsager Theory

Onsager predicted a simple model of lyotropic, entropy-driven phase transitions [**Onsager1949**]. Rod-like particles are modelled as thin spherocylinders with length L and ~~diameter~~ diamater D, and an excluded volume preventing overlap. The interaction potentials between ~~the particles~~ the particles are neglected, and only the configurational entropy of the system considered. Qualitatively, the confinement of rods ~~parallel to a director $\vec{n}$~~ parallel to a director $\vec{n}$, such as in the nematic phase, leads to a decrease in ~~rotational~~ rotational entropy, but an increase in ~~translational entropy allowing rods to move freely~~

~~parallel to each other~~transltional entropy allowing rods to move parallel to each other. At sufficiently high concentrations, the ~~translational~~ rotational entropy will dominate, and the system ~~undergoes~~ undergo a phase transition from isotropic to nematic.

The critical volume fraction at transition is approximately $4r/L$, where r is the radius of the rigid rod, and L its length (see Appendix A). This means the isotropic–nematic phase transition occurs at lower concentrations for mesogens with greater aspect ratio, and requires a minimum aspect ratio of $L/r = 4$ to occur. It is worth noting that this result is only valid in the limit of thin spherocylinders, as Onsager's derivation neglects Virial coeffecients B_n beyond second order in the expansion of the free energy in powers of density [**Frenkel1987**], ~~as discussed in Appendix A~~as discussed in Appendix A. Onsager's theory has since been tested, with both computational [**Frenkel1987b**, **Frenkel1988b**] and experimental [**Kubo1979**, **Oldenbourg1988**, **Fraden1993**] results substantiating its validity.

2.3 Order Parameter

The degree of order in a liquid crystal phase is characterised by an order parameter, chosen such that it ~~is unity in the fully ordered phase and zero in the isotropic phase. An example is the magnetisation **M**~~ is $S = 1$ in the fully ordered and zero the isotropic phase. An example is the magnetisation **M** of a ferromagnet; when raised above a critical temperature, the magnetisation vanishes as the ferromagnet undergoes a phase transition. While the choice of order parameter for the nematic phase transition is less intuitive than this, it relies on the formation of genuine long-range orientational order. We may therefore define the angle (θ) between each molecule's axis and the system ~~director, such that the nematic order parameter S_n can be written as:~~ director, such that the order parameter S can be written as:

$$S_n = \langle P_2(\cos(\theta)) \rangle = \left\langle \frac{3}{2}\cos^2(\theta) - \frac{1}{2} \right\rangle, \tag{1}$$

where P_2 denotes the second Legendre polynomial [**DeGennes1993**]. While $\langle \cos^2(\theta) \rangle$ would function alone as the order parameter, ~~this confines S_n to values between unity for a perfectly aligned system, and zero for a completely random system. Further information on the motivation behind this choice, and how it is implemented in our simulation, is given in Appendix ??~~this confines S_n to values between unity for a p Appendix B.1.

Similarly, ~~it is helpful to define~~ it is helpful to define a smectic order parameter S_s, to characterise the formation of one-dimensional long-range positional order. ~~We can expect~~ We can expect a non-zero Fourier component of the normalised density along the director [**Polson1997**], and so ~~can write:~~ we can write

$$S_s = \frac{1}{N}\left| \sum_{j=1}^{N} \exp\left(\frac{2\pi}{L} i \mathbf{r}_j \cdot \hat{\boldsymbol{n}} \right) \right| \tag{2}$$

for layers of periodicity L perpendicular to the nematic director $\hat{\boldsymbol{n}}$, and where $\mathbf{r}_j$ denotes the centre of mass position of the jth molecule [**Dussi2018**].

2.4 DNA as a Liquid Crystal

Lyotropic liquid-crystalline phases are very common in living systems, from cellular membranes to fibroblast structures [**Stewart1966**, **Rey2013**]. In vitro, many biochemical molecules such as cellulose, peptides, and protein assemblies have also been shown to form liquid crystal states [**Zhao2019**]. With respect to the mesogenic behaviour of DNA, Luzzati et al. first observed a columnar phase in a condensed DNA solution in 1959 (only 6 years after the discovery of the double-helix structure), and Robinson pioneered the development of the twisted-nematic phase in 1961 [**Luzzati1959**, **Robinson1961**]. Subsequent work by Strzelecka et al. has demonstrated experimentally that DNA molecules can form precholestric, cholestric and smectic phases (in order of increasing concentration) though lyotropic phase transitions [**Strzelecka1988**].

Returning to Onsager's theory, with the known dimensions of DNA we find that that the minimum base pair length required to obtain liquid crystalline phase behaviour is 24 base pairs [**Bolhuis1997**]. However this limit has been broken experimentally by Nakata et al. [**Nakata2007**, **Zanchetta2008**], which they suggest is a result of monomer stacking through end-to-end adhesion to form the larger mesogens required.

These techniques may be applied to developing DNA origami, the process whereby complex nano-structures are constructed out of DNA molecules. Though a greater understanding of the phase behaviour of DNA nanoparticles, we may inform design of more complex structures, and develop colloidal self-assembly processes. These techniques may have applications in biophysics, photonics, structural biology, and synthetic biology [**Nummelin2018**, **Praetorius2017**, **Bathe2017**].

2.5   Previous Simulation Work

Computational work may be implemented over a broad spectrum of coarse-graining (a process whereby microscopic degrees of freedom are integrated over to reduce the computational costs of a simulation at the cost of lower model resolution), where the base unit of the simulation ranges from single atoms to large bulk molecules [**Inglfsson2013**, **Potoyan2012**]. Atomistic models, such as CHARMM [**MacKerell1995**] and AMBER [**SalomonFerrer2012**], offer ~~the~~ a greater level of detail, but are limited by computational cost beyond small (>30 base pairs) models [**Cheatham2004**]. In contrast, bead-spring polymer models (with up to 3000 base pairs per bead) may obtain bulk material properties at significantly lower computational expense [**Michieletto2016**].

Such models have been applied specifically to DNA nunchucks by Salamonczyk et al. [**Salamonczyk2016**] to suggest the existence of smectic phases. However, this is limited by the level of coarse-graining applied, as the artificial interaction potentials considered have no physical origin. This project work builds on this research, by applying a intra-molecular potential derived by single nucleotide simulations of the nunchuck molecule by Jiaming Yu (within the Eiser Group) using OxDNA, a lower-level coarse grained model that accurately represents the physical properties of single and double stranded DNA [**OxDNA**].

My work is based on a coarse-grained model developed by Xing et al. [**Xing2019**] to consider Y-shaped nanoparticles constructed from DNA, utilising LAMMPS [**LAMMPS**], a ~~software package~~ software-package to model dense systems of these nunchuck nanoparticles. This ~~approach allows us to simulate larger systems of DNA-mesogens, and provides~~ approach allows us to simulate larger systems of DNA-mesogens, and provides a better predictor of this system"'s experimental phase behaviour.

3   Methods

~~All molecular dynamics (MD) simulations presented here were completed in LAMMPS (Large-scale Atomic/Molecular Massively Parallel Simulator), a medium coarse-grained, MD code~~ All molecular dynamics (MD) simulations presented here were completed in LAMMPS (Large-scale Atomic/Molecular Massively Parallel Simulator), a medium coarse-grained, MD code developed to replicate solid-state materials and soft matter mesoscopic systems [**Plimpton1995**, **LAMMPS**].

3.1   Simulation Molecules

~~Here~~Here, we are considering 'nunchuck' molecules formed of two rigid rods connected by a flexible linker, as depicted in Figure 2a. ~~As~~ As the interaction potential of an anisotropic particle is rather complex, it is computationally simpler to consider each molecule as a system of connected spheres, each with a separate isotropic interaction potential (detailed further in Section 3.3).

This is visualised in Figure 2b, for rigid arms of aspect ratio 7. The ss-DNA is represented by a further sphere in the centre of the molecule, coloured red to highlight its differing mechanical properties. It has a modified bond angle, so the molecule is bent around this element, and reduced bond rigidity so the particle may also stretch about this point. We also consider a simplified system of rigid rods with no modifications on the central atom, to verify the analysis methods against known results.

(a) *Coarse-grained Model*

(b) *LAMMPS Implementation*
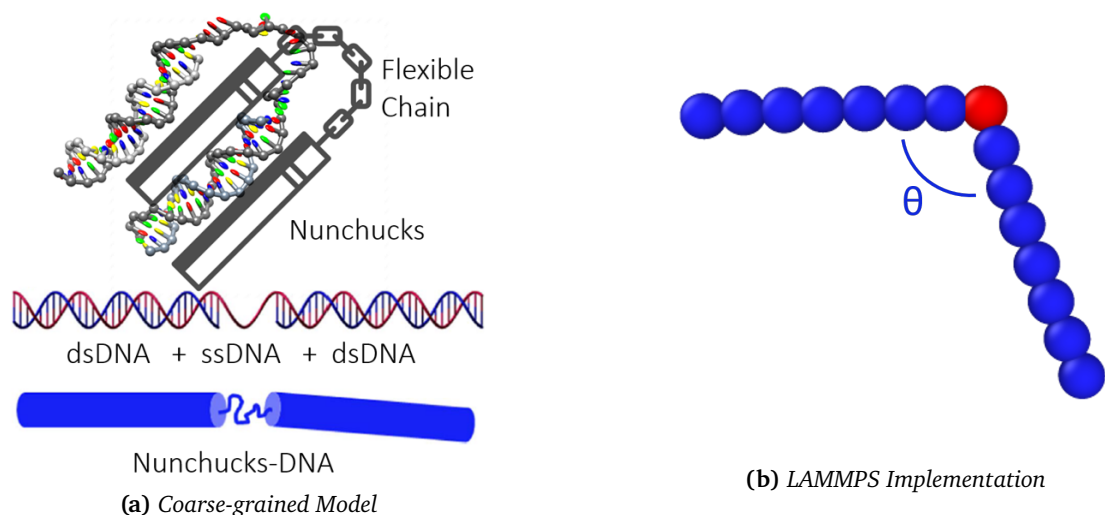
Figure 2: *Depiction analogy between the DNA mesogen and the nunchucks. Note the appearance of the flexible ss-DNA linker between the rigid ds-DNA rods, and the implementation within LAMMPS on the right. The central red sphere, representing the ss-DNA, is given modified bond properties to replicate the nunchuck's flexibility. Figure (a) created by Jiaming Yu (Eiser Group, Cambridge).*

A system of natural units was used in simulations, and replicated in our results here. Based on the Lennard-Jones potential, the cut-off length and characteristic energy are both set to unity. The simulation timescale is then fixed by the choice of these values, and the mass of the simulation body.

The physical values for a system may be considered for a specific system (in this case strands of ds-DNA) through scaling via the relevant mass, length scale and energy scale of this system. However the dimensionless simulations presented here may be generalised to any similarly-shaped mesogens; we would expect other systems to display the same behaviour over an appropriate timescale determined by their material properties [**Rapaport2004**].

For the nunchuck particles considered, a length scale of $2\,\mathrm{nm}$ is used (corresponding to the width of ds-DNA, and hence the diameter of a simulation sphere) [**Arnott1972**]. It is worth noting that the persistence length of DNA is around $50\,\mathrm{nm}$ [**Garcia2007**], so the approximation of perfect rigidity is valid for all rods considered here (maximum length $30\,\mathrm{nm}$). Using the standard value of $0.33\,\mathrm{nm}$ [**Langridge1960**] for the average length of a base pair, each sphere corresponds to a sequence of six base pairs. This gives the mass of each sphere as $6.5 \times 10^{-24}\,\mathrm{kg}$, based on an average formula mass per base pair of $650\,\mathrm{Da}$ [**Duewer2018**]).

We may also define the characteristic energy scale; this is formally the depth of the potential well in the full Lennard-Jones potential, but the thermal energy serves as a common approximation [**Pan2010**] in agreement with experimental data [**Wang2002**]. Using these values, we find that the characteristic timescale for this system is $79\,\mathrm{ps}$. In this context, the simulation timestep would be $0.4\,\mathrm{ps}$, and typical simulation of 20×10^6 steps had a total duration of $7.9\,\mathrm{\mu s}$. For 1000 particles, this took approximately 8 hours to run on a standard laptop CPU.

3.2 Simulation Structure

All simulations in this report were conducted for a system of 1000 particles, with a time step of 0.005τ, (where τ is the characteristic time), unless otherwise stated. The system was initially configured in a dilute, isotropic state; a non-trivial process for large numbers of mesogens as molecules must be placed randomly without overlap, to prevent any initial order affecting the ~~subsequent~~ subsequent formation of ordered phases. ~~When studying high volume fractions, simulations were~~ I thank Iria Pantazi for writing a python script to automate this process for dilute rigid rod systems, and a generalised version of this is available in the supplementary material. When studying high volume fractions, simulations were also

initiated from a perfectly ordered square crystalline phase, with all molecules aligned along a common axis. The choice of this axis is arbitrary, as the system is invariant under global rotation [**Nos1983**], but is taken to be directed along the ~~y~~ y-axis for clarity. Care was taken to ensure molecules did not overlap, and ~~that~~ that the system was stable in this ordered phase.

All simulations are conducted within an oblong box defined by the Cartesian axes, with periodic boundary conditions [**Frenkel2002**]. The aspect ratio of this box may be varied, to support phase formation in anisotropic systems, as discussed in Section ~~5.3~~X. An isenthalpic ensemble was used (where pressure is fixed) to vary the size of the simulation region (either contracting or expanding), allowing sampling of different volume fractions from the same initial configuration. The microcanonical ~~(N, V, E) ensemble, with conserved volume and energy,~~ (N, V, E) ensemble, with conserved volume and energy, was then used to allow the system to reach thermodynamic equilibrium. Time integration was evaluated using the Nose-Hoover thermostat [**Nos1984**, **Hoover1985**] natively implemented in LAMMPS [**Shinoda2004**], with a damping time of τ.

A typical simulation consists of multiple stages, alternating between these two ensembles to sample the system properties at a range of volume fractions. Approximately 2×10^4 steps are simulated when varying the simulation volume (depending on the resolution of volume fraction sampling), followed by 2×10^6 ~~steps allowing the system to reach equilibrium in each stage~~ steps, allowing the system to reach equilibrium. The output of thermodynamic variables, as well as particle positions, at the end of each stage allows for subsequent calculation of the order parameter at equilibrium. ~~These data were~~ These data were retrieved at regular intervals during each simulation stage, to track the time evolution of the system.

To ensure stability of the system, a Langevin thermostat [**Schneider1978**] was also used throughout, and energy conservation was verified over a range of timescales. The damping for all thermostats is equal to the characteristic timescale of the simulation (i.e. unity in natural units).

3.3 Intermolecular Potential

A shifted, cut-off Lennard-Jones potential was chosen to represent pair-wise interactions between molecules. While the Lennard-Jones potential [**Jones1924a**, **Jones1924b**] has long been the natural choice for molecular dynamics simulations [**Stephan2019**], its infinite range introduces computational complexity as interactions between all pairs of particles must be considered. It is therefore increasingly common to use a cut-off version, whereby the potential is set to zero beyond a 'cut-off' radius, and here we chose to neglect the entire attractive tail. As well as simplifying the calculations required, this also allows our results to be generalised to any mesogens without attractive inter-molecular forces (that typically favour ordered-phase formation), as any phase transitions observed here must be purely ~~entropy-driven~~ entropically driven. This is commonly known as a soft-core model, where particle overlap is suppressed via this repulsive potential rather than any excluded volume interactions, and is computationally much less demanding [**Paolini1993**, **Hughes2008**].

However, this cut-off may cause unphysical behaviour if the potential does not tend to zero smoothly. This is remedied by the addition of a constant term, described in the full form of the pair-wise potential U_{ij} in (3):

$$U_{ij} = 4\epsilon \left[\left(\frac{\sigma}{r_{ij}} \right)^{12} - \left(\frac{\sigma}{r_{ij}} \right)^6 \right] + \epsilon \qquad r_{ij} < r_c = 2^{1/6}\sigma \tag{3}$$

Here σ and ϵ are the relevant length and energy scales of the system, formally corresponding to the particle separation at which the $U_{ij} = 0$, and the depth of the potential well. It is worth noting that the effects of this truncation and shift on the overall thermodynamic quantities are well documented [**Stephan2020**, **Shaul2010**], and changes in lyotropic properties are negligible in 3D bulk liquids with a conserved particle number [**Smit1991**]. This purely repulsive potential is also a good representation of the physical DNA system considered here ~~, due to the effects of Debye screening~~ [**Strey1997**, **Strey1998**].

3.4 Analysis Methods

We employed the visualisation freeware Ovito [**Ovito**] to animate the mesogens motion, and was used to generate all particle images presented here. Thermodynamic variables, such as internal energy and pressure, were extracted to track the system's progress towards equilibrium, and verify its stability.

The volume fraction and nematic order parameter were computed for comparison with Onsager's theorem, as detailed in Section 2.2. Calculation of the order parameter is complicated by the absence of an imposed director (i.e. if no electric field is applied), and we use the approach taken by Eppenga and Frenkel [**Eppenga1984**] which is reproduced in Appendix B.2.

Further analysis included the calculation of the smectic order parameter, and pair-wise orientational correlation coefficient, detailed in Section 5.3. All scripts for data extraction and analysis were written by the author, and is attached as supplementary material.

4 Rigid Rod Simulations

First we studied a system of rigid rods to verify that the analysis methods we employed were able to reproduce Onsager's theory. We focused specifically on the isotropic-to-nematic phase transition, as it is well studied, and verified computationally through both Monte Carlo (MC) [**Frenkel1984, Lee1987**] and MD simulations [**Allen1987, Camp1996**].

First we studied a system of rigid rods to verify that the analysis methods we employed was able to reproduce

4.1 Shrinking the Simulation Box

For rigid rods with an aspect ratio $L/D = 10$, Onsager's theory predicts a lyotropic phase transition at a critical volume fraction of $\phi = 0.4$. Considering a system of rigid rods, formed of sequentially connected 'balls' (force-centres), we applied alternating stages of contraction (increasing the volume fraction) and equilibration steps (keeping the volume constant). Onsager's theory predicts a lyotropic phase transition at a critica Each contraction stage consists of between 1×10^4 and 5×10^4 steps (chosen to identify the critical volume fraction with maximal resolution, while verifying the order parameter is approximately constant outside of this), while the equilibration stage runs for 2×10^6 steps. In this way we are able to confine the possible critical volume fraction to the range $0.39 < \phi < 0.44$, as observed in Figure 3, in good agreement with Onsager's prediction.

This analysis was repeated for longer rods with an aspect ratio of was repeated for longer rods with an aspect rat 16, and a predicted critical volume fraction of $\phi = 0.25$. My simulations verified that the critical volume fraction lies in the range $0.23 < \phi < 0.26$, in good agreement with theory My simulations verified that the critical vol This also provides a useful example of the characterisation of a phase transition through changes in the thermodynamic variables; Figure 4 depicts a change in pressure during the equilibration stage, corresponding to the isotropic–nematic phase transition.

4.2 Expanding Simulations

We also consider the phase behaviour upon expansion from a perfectly ordered state, in hope of observing the same phase behaviour, as would be expected for an equilibrium system expected for an equilibrium system. This has two advantages; it allows us to access higher volume fractions that are not easily accessible through the shrinking procedure, and also provides verification of the phase transitions previously observed. Ensuring a novel phase is in true equilibrium has long been the bane of liquid crystal simulators, however, non-equilibrium effects will manifest themselves in a hysteresis of the phase transition (variation in the critical volume fraction dependant on the direction of the transition), and so can be easily identified through this method.
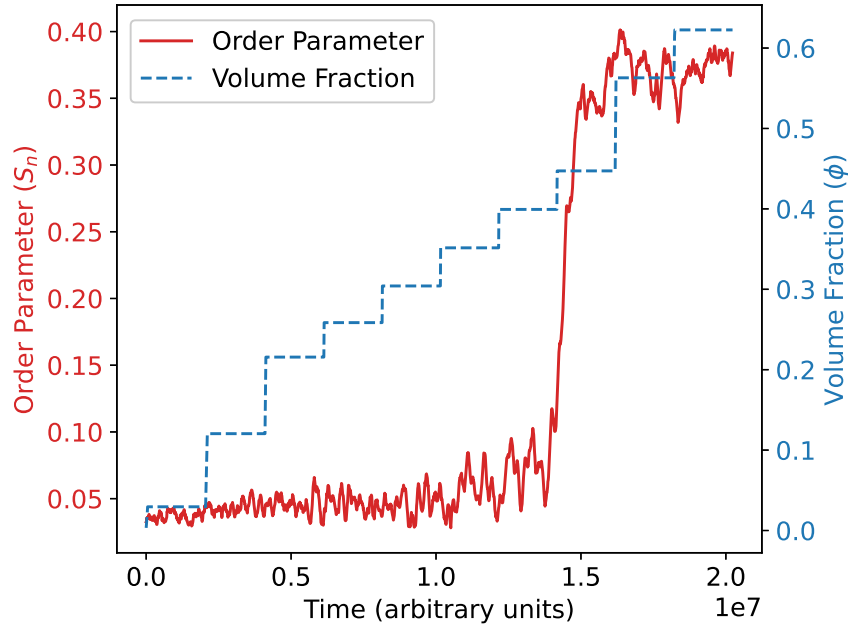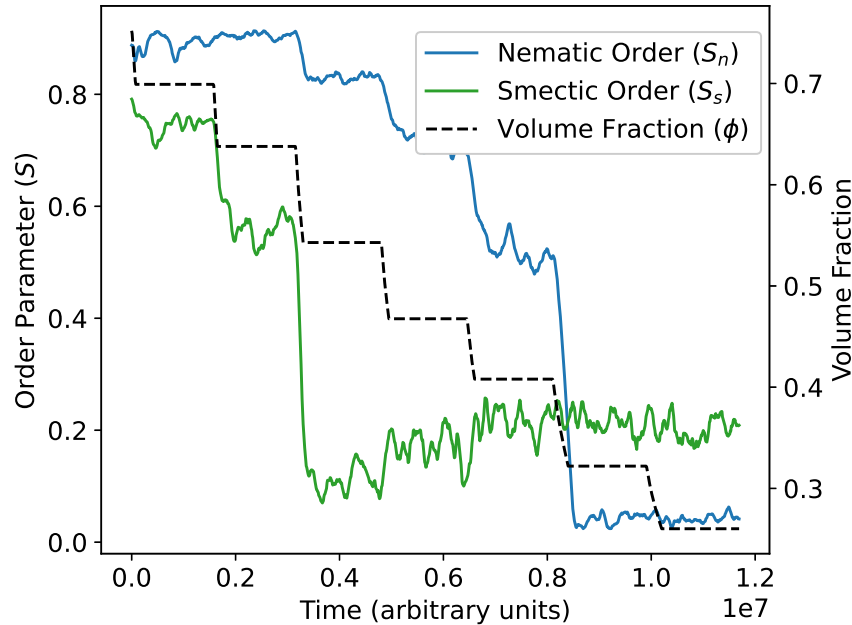
Figure 3: *The evolution of the volume fraction and the nematic order parameter over the timescale of the simulation, for a system of 1000 rigid rods with aspect ratio 10. The jump in S_n (red line) occurs at about $\phi \sim 0.4$ The evolution of the volume fraction and the nematic order parameter over the timescale of the simulation, for that the contraction steps, where the volume fraction is increased, are not of equal durations, and so do not correspond to equal changes in the system volume; rather they are chosen to highlight the phase transition. The contraction period is much shorter than the equilibration time, but the changes in volume fraction are not instantaneous, despite their appearance here.*
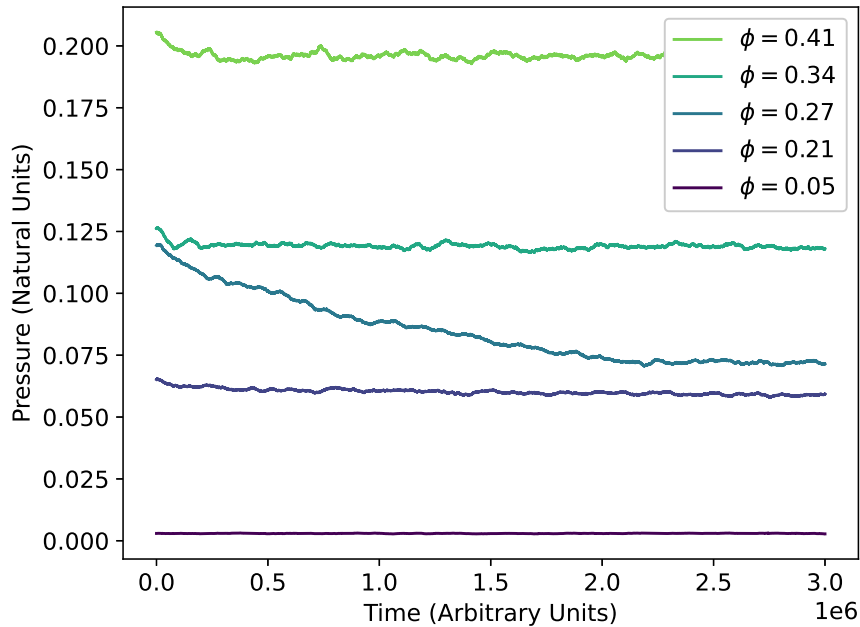
Figure 4: *The evolution of pressure on subsequent microcanonical ensembles (between which volume is decreased), when simulating 1000 rigid rods of aspect ratio 16. Note the extended decay in pressure for $\phi = 0.27$, while the isotropic–nematic phase transition occurs; all other stages remain at equilibrium throughout.*

Initially, the particle force centres are placed on a simple cubic lattice. Again equilibration is run in the microcanonical constant volume and alternated by an isenthalpic ensemble, however the

particle-force centres are placed on a simple cubic lattice. Again equilibration is run in the microcanonical constan the target pressure for the Nose-Hoover thermostat is now reduced below the system pressure so that expansion occurs in these isenthalpic stages. The length of these stages is unchanged from Section 4, however, the thermostat damping is increased to 100τ to ensure stability of the expansion.


Figure 5: *The evolution of the volume fraction against both the nematic (S_n) and smectic (S_s) order parameters over the timescale of the simulation, for a system of 1000 rigid rods with aspect ratio 10 initiated in a crystalline phase. A continuous smectic–nematic phase transition is observed (in green) at high volume fractions, followed by a discrete nematic–isotropic transition (in blue), occurring when ϕ is decreased when ϕ decreased below 0.4. Note that there are multiple steps in the smectic order parameter, indicating this transition occurs over a range of volume fractions.*

The isotropic phase formation was observed in the region $0.38 < \phi < 0.41$, in good agreement with the results of Section 4, and confirming this is indeed an equilibrium phase transition.

The higher volume fractions accessed at the start of the simulation also give rise to another phase transition; forming this nematic phase from the initial ordered phase. While the system was configured in a crystalline phase, it quickly relaxes into an a smectic-like phase with the one-dimensional, long-range positional order. The subsequent smectic–nematic transition is then observed with a reduction in the smectic order parameter around $\phi = 0.6$, as shown as shown in Figure 5. This transition is clearly concentration-dependant (with discrete jumps in the order parameter when the volume fraction is reduced), however, it occurs over a range of volume fractions and so is likely a continuous phase transition. While our evidence here is not conclusive, this is still a matter of active research and beyond the scope of this report. Theoretical [**Wen1987**], computational [**Frenkel1988**, **McGrother1996**], and experimental [**Dogic1997**, **Doane1972**] evidence however suggests that this transition is expected to be continuous (or at most weakly first-order) for rigid rods of extended aspect ratios, and occurs around this volume fraction.

5   Nunchuck Simulations

Furthermore I applied the same simulation Further, I applied applied the same simulation approaches to the nunchuck molecules introduced in Section 3.1. These could be configured in two ways; either with a fixed angle between the two rigid arms, or a fixed rigidity (which determines the angular potential between the two arms, and hence the distribution of angles observed). Previous work by Jiaming Yu

(a) *Side View*   **(b)** *Perspective View*
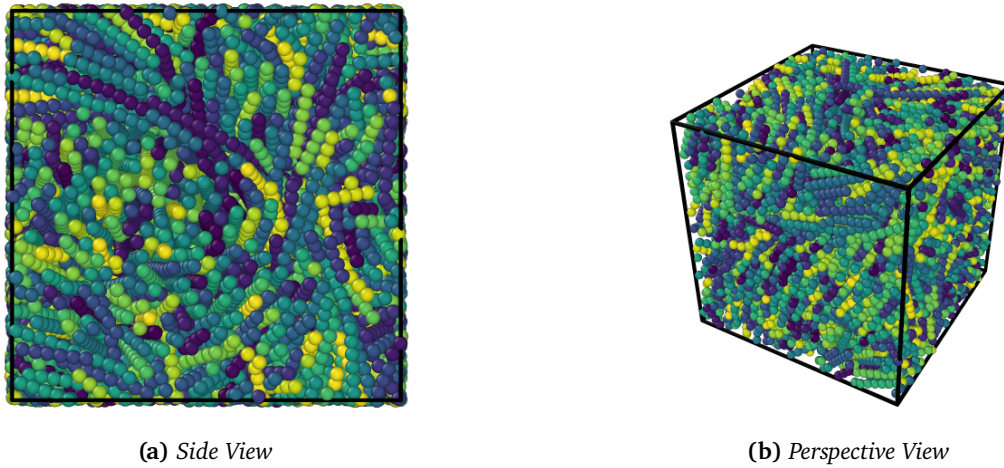
Figure 6: ~~*The quasi-ordered*~~ *Quasi-ordered phase formed by* 1000 *fully flexible nunchucks. Note the local regions of aligned rods, suggesting a nematic-like phase, but also the variation of the director across the sample (between these regions). The length scale of any periodicity in this variation is larger than the simulation box itself.*

using OxDNA [**OxDNA**] has suggested that the fixed rigidity model provides an accurate coarse-grained model of the DNA-nunchucks; however, the fixed angle approach is also used for simplicity, and because it appears more amenable to ordered phase formation.

5.1 Fixed Rigidity

Initially, nunchucks with complete bond flexibility are considered. Despite this, a nematic-like phase was observed at volume fractions $\phi > 0.4$, with a maximal order parameter of 0.6 comparable to those measured previously in rigid rod systems. Despite this, a uniform, system-wide director was not observed, with the preferential orientation varying across the simulation region ~~shown~~ shown in Figure 6.

Consideration of the distribution of nunchuck bond angles (i.e. the opening angle between the two rigid arms) confirmed the formation of an ordered phase, with a clear preferential angle forming in Figure 7. However, it is clear that any periodic variation of the director occurs on a length scale greater than the size of the simulation region, preventing further characterisation of this phase. Unfortunately, the computational resources required to simulate larger systems were beyond the scope of this project, due to the scaling of particle number over volume required to achieve the same density.

5.2 Fixed Angle

~~Therefore, I considered systems where the nunchuck opening angle is~~ Therefore, we considered systems for which th[e] confined to a particular value. ~~I suggest that, in comparison to the fixed rigidity case, quasi-nematic structures may be observed on shorter length scales, particularly when this opening angle is confined below the mean angle (see Figure 7)~~ We suggest that similar to the rigid-rods, quasi-nematic structures may be obs[erved] We tested phase formation over a wide range of rigid rod lengths and opening angle values; broadly we found that larger opening angles favoured nematic-like phase formation ~~(with a maximal order parameter of $S_n = 0.62$),~~ for which our analysis methods were best suited to identify, but smaller angles did not form obvious alternate ordered phases. Two such quasi-nematic phases observed are depicted in Figure 8.

Alongside the ~~tendency here to form a nematic phase with all molecules having a similar alignment along a constant global director~~ tendency here to form a nematic phase with all molecules having a similar alignme[nt] there appears to be more periodic ordering, such as the herringbone structure, which is clearly visible in Figure 8a, or the rotation of the system director across the sample in Figure 8b (typical of a twisted nematic phase). These structures cannot be described by our current order parameter methods.
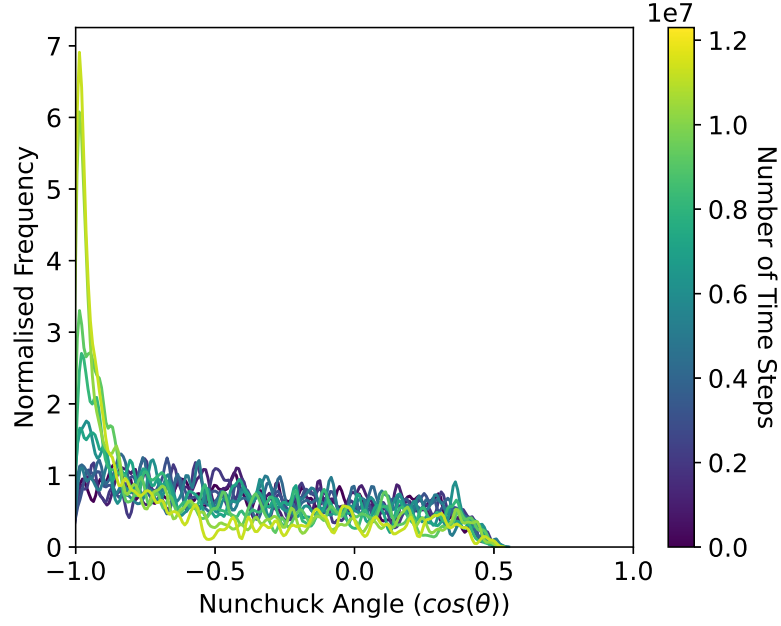
Figure 7: *A kernel density estimate plot of the distribution of nunchuck opening angle (between the two rigid arms) over time (as the volume fraction is reduced), where nunchucks are completely flexible. Plotted for a system of 1000 particles, with the distribution sampled every 1×10^6 time steps. Note the formation of a preferential angle at late times, corresponding to the formation of an ordered phase at high volume fractions.*

5.3 Orientational Order Parameter

Alternative methods to characterise the order of the system are typically motivated by the class of symmetry expected. Given that our system appears to display a degree of orientational order, a length-dependant orientational order parameter is introduced to verify this order is truly long-ranged and not simply due to short range steric effects. This also allows the identification of any periodic aspects to the system as oscillatory components in the order parameter.

We consider an l-th rank pair-wise correlation function, where $g_l(r)$ gives the correlation between the orientation of two particles separated by a distance r

$$g_l(r) = \frac{\langle P_l(\hat{\boldsymbol{u}}_{\boldsymbol{i}} \cdot \hat{\boldsymbol{u}}_{\boldsymbol{j}})\delta(r_{ij} - r)\rangle}{\langle \delta(r_{ij} - r)\rangle}, \tag{4}$$
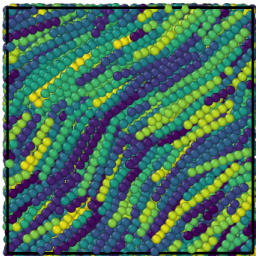
(a) *Herringbone Structure*
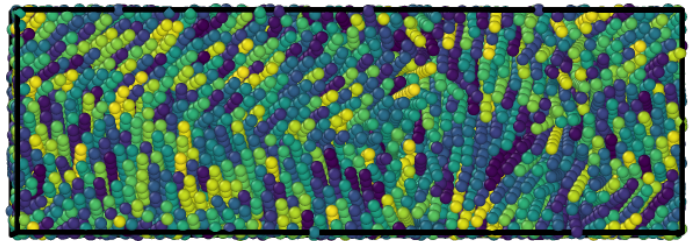
(b) *Twisted Nematic Structure*

Figure 8: *Two ordered phases formed separately by 1000 nunchucks with an opening angle of 150°. Note the global alignment of molecule directors, giving a high nematic order parameter in either case. An alternating herringbone-like structure in observed in **(a)**, while the direction of the system director varies across the length of the simulation region in **(b)**, akin to a twisted nematic phase.*

where $\hat{\boldsymbol{u}}_i$ is the director for molecule i, and r_{ij} is the separation between a given pair of molecules i and j [**Zannoni1979**]. In the disordered phase, this ~~pair-correlation function~~ pair-correlation function decays to zero, while in the ordered phase it decays to the square of the orientational order parameter [**Frenkel1985b**]:

$$\lim_{r \to \infty} g_l(r) = \langle P_l \rangle^2 . \tag{5}$$

Details of the simulation methods of $g_l(r)$ are given in Appendix B.3.

This may be applied to the systems ~~shown in Figure 8. However~~ shown in Figure 8. However, this approach is limited by the length scale of the simulation region; the maximum separation between particles is half the size of the simulation region due to the periodic boundary conditions [**Frenkel1985c**].

To determine order over longer length scales, without increasing the volume of the system (due to the limited computational resources), we instead vary the aspect ratio of the system. By considering an elongated oblong simulation region, such as in Figure 8b, we are able to sample correlations over longer distances (along the long axis of the box) for systems of the same particle number. Using this method, ~~the curves in Figure 9 confirm~~ the curves in Figure 9 confirm that the order observed in this fixed angle system is indeed long-range, with a non-decaying correlation at long length scales.
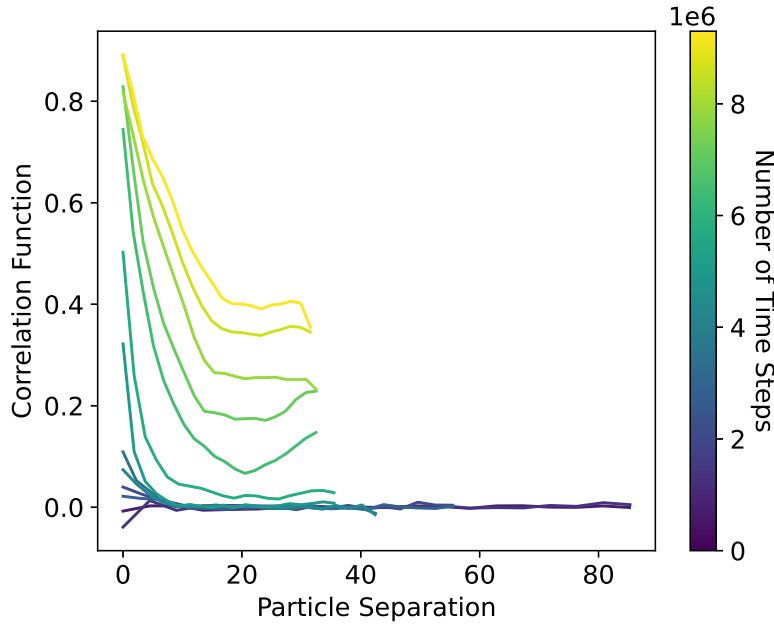
Figure 9: *Orientational correlation function over time (as the volume fraction is reduced), where nunchucks have a fixed opening angle (between the rigid arms). Plotted for a system ofXX*

This method is limited by the use of a single vector along the molecular axis to define the orientation of the molecule; two vectors are required to uniquely specify the orientation of a single nunchuck molecule. Using the molecular axis alone only accounts for quasi-nematic order; and does not consider any biaxial or herringbone substructure. We therefore also consider additional orientational correlation functions for the bisector of each molecule, and normal vector to the plane of the nunchuck. The first Legendre polynomial is used for the bisector to detect changes in sign of the bisector direction, as would be expected in a herringbone structure.

However, no statistically significant periodic components in the correlation function were observed over the length scale of the simulation region. A visual inspection of Figure 8 suggests that the ~~length of the~~ simulation region is approximately ~~half~~ a factor two shorter than the full period of the repeating structure, and so further research on larger simulation regions is required to verify these phases.

6 Dynamic Properties

While the phase behaviour of rigid rods is well studied, much less is known about the dynamical properties of the individual mesogens inside these quasi-rdered p This in, in part, due to the traditional popularity of using MC approaches, which cannot predict dynamic properties. Despite this, this MC approach has enjoyed a more recent popularity in both computational and experimental studies [**GayBalmaz2013**, **Zhao2013**, **Rey2013**]. Here, we undertake a brief study into the dynamical properties of the nunchuck system, and demonstrate the application of dynamical properties to static phase identification. In particular, we focus on the diffusion coefficient D defined by the evolution of the mean-squared displacement (MSD) as function of time t in d dimensions:

$$\left\langle (x(t) - x_0)^2 \right\rangle = 2dDt \tag{6}$$

A derivation of this result is given in Appendix C. It is also instructive to consider the 'power-law' formation of this relation [**Ernst2013**]:

$$\left\langle (x(t) - x_0)^2 \right\rangle = 2dD_\alpha t^\alpha \tag{7}$$

which reduces to the pure-diffusive case of (6) when $\alpha = 1$. Otherwise the process is characterised as subdiffusive ($\alpha < 1$) or superdiffusive ($\alpha > 1$) [**Metzler2000**]. Displacements were only sampled over equilibration phases of our simulation, and the effect of the periodic boundary conditions were explicitly accounted for by offsetting additional displacements from boundary crossings. Linear regression analysis was used to predict the value of α for each run, over a variety of volume fractions in the dilute limit. This limit occurs when each particle may exist in a non-overlapping free volume of rotation (a sphere circumscribed around the molecule), at a maximal volume fraction of

$$\phi_{dilute} = \frac{\pi(D/2)^2 L}{\frac{4}{3}(L/2)^3} = \frac{3}{2}\left(\frac{D}{L}\right)^2 . \tag{8}$$

For rigid rods with an aspect ratio of 10, this gives a value of $\phi_d = 0.015$. We find an average power of $\alpha = 0.97 \pm 0.03$ for the nunchuck molecules, and $\alpha = 1.00 \pm 0.04$ for the rigid rods, as expected for diffusive behaviour.

As the volume fraction is increased, we observe a tendency towards subdiffusive behaviour, with a reduction in the value of α. This is given by the gradient when the root mean-squared (RMS) displacement is plotted over time in logarithmic space, as best demonstrated in Figure 10. This depicts coordinate-wise displacement across three different phase regimes, for a system of rigid rods. Here, the Cartesian axes may be used, as simulations are configured in a crystalline phase with molecules orientated along the y-axis, and smectic layers forming in the $x - z$ plane. Phase transitions for this system have previously been identified in the regions $0.58 < \phi < 0.62$ for the smectic–nematic and $0.38 < \phi < 0.43$ for the nematic–isotropic transition.

At the highest volume fractions ($\phi \geq 0.62$), the diffusion along the y-axis is significantly reduced, due to the restricted motion between layers in the smectic phase. Below this, a nematic phase is observed, with increased diffusivity along the molecule's director (aligned with the y-axis) corresponding to an increased intercept in logarithmic space. At the lowest volume fractions ($\phi \leq 0.38$), there is no preferred direction in the system and diffusion is completely isotropic. Particle motion in the x- and z-axis is approximately diffusive throughout (ie $\alpha = 1$), but the lower intercept at higher volume fractions corresponds to a reduced diffusion coefficient.
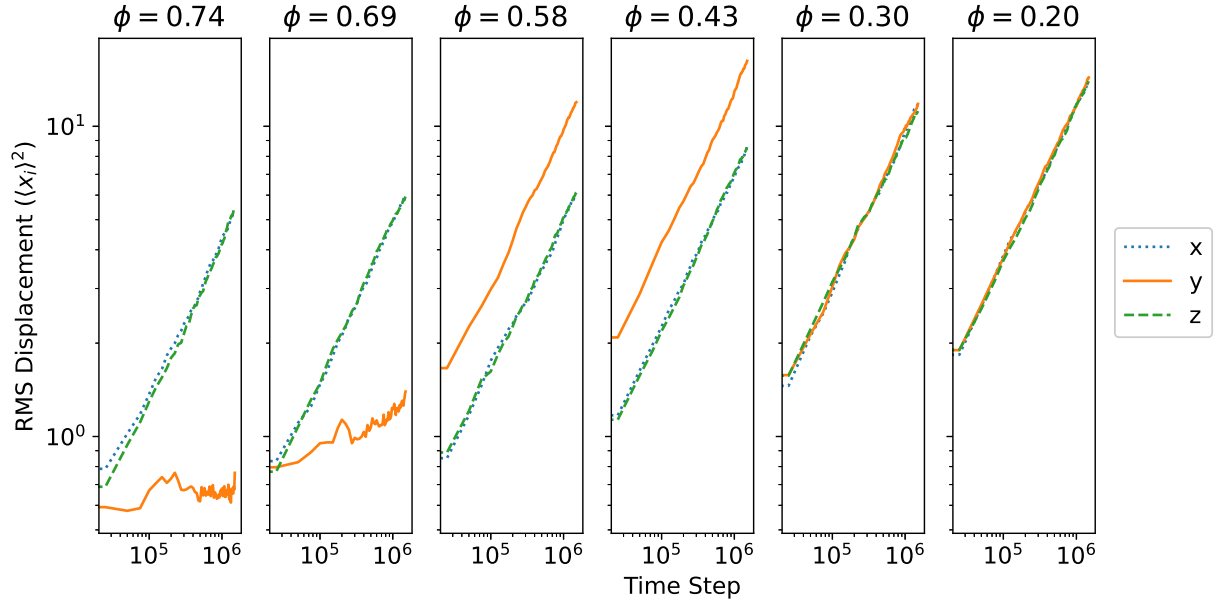
Figure 10: *Root ~~mean squared displacement~~ <ins>mean-squared displacements</ins> against time in a system of 1000 rigid rods <ins>with an aspect ratio 10</ins>, for a range of volume fractions ϕ. The leftmost pair of plots correspond to the smectic phase, with restricted motion between $x - z$ layers along the y-axis. The centre pair give the nematic phase, with preferential displacement along the ~~y axis~~ <ins>y-axis</ins>. Finally, the rightmost pair give the isotropic phase, with no preferential direction and isotropic diffusion. Note that there are no significant differences between the x- and z ~~directions~~ <ins>-directions</ins> in any phase, as these directions are equivalent in the phase structure.*

Phase formation may also be observed through deviations in these coordinate-specific diffusion coefficients. Applying this to the ~~nunchucks~~ <ins>nunchuck</ins> system, isotropic diffusion is observed at low volume fractions in Figure 11~~. However, ~~<ins>, but</ins> the y-coordinate diffusion coefficient is severely reduced ~~beyond this, with an maximal anisotropy of $D_y/D_x = 0.19$ at $\phi = 0.58$~~<ins>before this</ins>. This strongly ~~indicates the onset of formation of the~~ <ins>hints towards the presence of a</ins> smectic phase below $\phi = 0.45$, in agreement with the prediction of $0.40 < \phi^* < 0.44$ obtained from the smectic order parameter. There is also some indication of the crystalline phase at the highest volume fractions, with diffusion equally limited in all directions, but this evidence is not conclusive.

7 Conclusion

We considered the phase behaviour of DNA nunchuck molecules, consisting of two sections of ds-DNA connected by a short section of ss-DNA. We introduced a coarse-grained model of DNA nunchuck particles, formed of two rigid rods connected by a (semi-) flexible linker, with soft-core purely repulsive potential interactions. We also introduced a simpler 'rigid rod' model, without the flexible linker, to verify the phase identification techniques used here.

~~Simulations of rigid rods demonstrated the existence of a first-order isotropic–nematic phase transition, and verified Onsager's across a range of aspect ratios. Within this, we confined the critical volume fraction for rods of aspect ratio $D/L = 10$ to the range $0.39 < \phi < 0.44$, in good agreement with the theoretical value of $\phi = 0.4$. We considered simulations sampling decreasing volume fractions from an initial crystalline phase, which confirmed the value of this critical volume fraction, verifying the transition occurred at true equilibrium by eliminating the possibility of phase hysteresis here. We also identified the formation of a smectic phase here,~~ <ins>My simulations of rigid rods were consistent with Onsager's predic</ins> however further categorisation of the transitions associated with this phase is left for a separate work.

Application of the same techniques to the ~~nunchucks system gave incontrovertible~~ <ins>nunchuck system</ins>
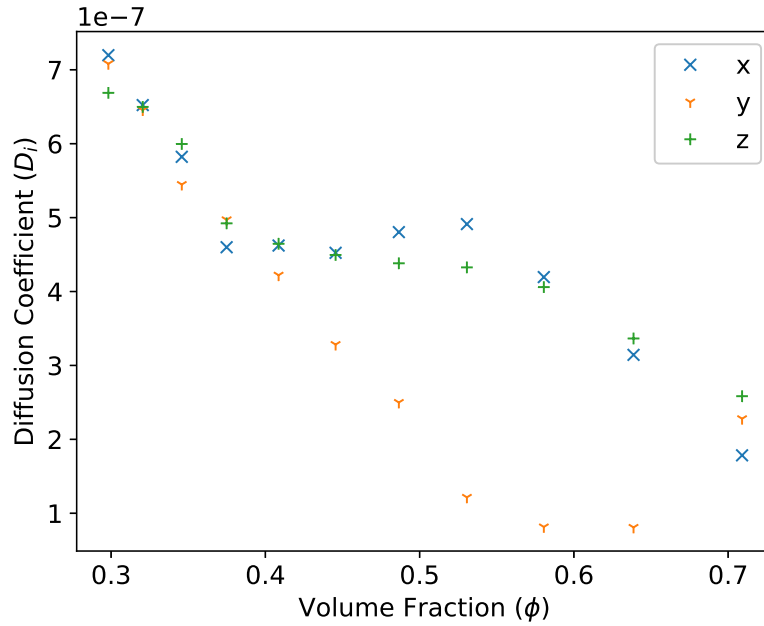
Figure 11: *Coordinate diffusion coefficients for the evolution of the microcanonical ensemble under a range of volume fractions ϕ. The low volume fraction region on the left of the graph corresponds to the isotropic phase, with no variation between coordinate axes. By contrast, the smectic phase in the high volume fraction gives rise to anisotropy in the coordinate diffusion coefficients, with reduced diffusivity perpendicular to the smectic layers in the y axis direction.*

gave evidence for the formation of an ordered, quasi-nematic phase in this system, in both the fixed rigidity ($S_n = 0.58$) and fixed angle ($S_n = 0.62$) configurations. The fixed rigidity configuration, a better representation of the ~~true~~ more realistic DNA system, demonstrated clear evidence for an ~~entropy-driven~~ entropy–driven phase transition, through the reduction in configurational entropy associated with the formation of a preferred angle. However, further analysis of this system suggested that any periodic order (associated with a novel phase) occurred on a length scale greater than could be simulated here, due to the associated computational costs.

In the fixed angle case, we subsequently introduced the orientational correlation function in order to identify any periodic order in the 'herringbone-like' and '~~twisted-nematic~~twisted' quasi-nematic phases observed. While this confirmed the presence of long-range order, we were unable to observe any periodicity here; we ~~suggest~~ believe that simulations of larger systems will be required due to the expected length scale of such periodic features.

Finally, we demonstrate that the measurement of dynamic properties provide a little-studied, alternative method to identify phase transitions and characteristic symmetries of such systems, in comparison with phases previously identified in both the rigid ~~rods and nunchucks systempreviously considered. We consider in particular~~ rod and nunchuck systems. In particular, I considered the formation of anisotropic phases through the variation in coordinate diffusion coefficients, such as in the smectic phase~~where the diffusion coefficient~~, where the diffusion coefficient of the mesogens within the ordered layers is up to a factor ~~of~~ 5.15 greater than between them. Further research is necessary to extend this beyond the simple Cartesian approach taken here, to allow the identification of novel phases, where the global director or symmetry class is not known. ~~Recent results~~ Results, I obtained only very recently, on directional diffusion within the ~~nunchucks~~ nunchuck system also suggest the formation of a novel biaxial phase ~~, and~~ – we are preparing a ~~separate publication on this~~publication on these.

Acknowledgements

Appendix A   Onsager Theory

A detailed and accessible derivation is provided by Doi and Edwards [**Doi1988**], and is not replicated in full here. Briefly summarising their method, the free energy of the system is initially expanded in powers of concentration ν, and higher order terms neglected to give the form:

$$\mathcal{A}[\Psi(\boldsymbol{u})] = \nu k_B T \left[\ln \nu - 1 + \int d\boldsymbol{u}\Psi(\boldsymbol{u}) \ln \Psi(\boldsymbol{u}) + \frac{1}{2} \int d\boldsymbol{u} \int d\boldsymbol{u}' \Psi(\boldsymbol{u})\Psi(\boldsymbol{u}')\beta(\boldsymbol{u}, \boldsymbol{u}') \right] \qquad (9)$$

where, for rigid rod-like polymers of diameter D and length L, $\beta(\boldsymbol{u}, \boldsymbol{u}')$ is given by:

$$\beta(\boldsymbol{u}, \boldsymbol{u}') = 2DL^2 \left| \boldsymbol{u} \times \boldsymbol{u}' \right| \qquad (10)$$

This expression may be minimised through the use of a Lagrange multiplier, giving a nonlinear integral equation that cannot be solved linearly. Onsager therefore assumed an equilibrium distribution of the form:

$$\Psi(\boldsymbol{u}) = \frac{\alpha}{4\pi \sinh \alpha} \cosh(\alpha \boldsymbol{u} \cdot \boldsymbol{n}) \qquad (11)$$

for molecule direction $\boldsymbol{u}$, arbitrary unit vector $\boldsymbol{n}$ and order parameter α determined by minimising the free energy. When the concentration exceeds a critical value ν^*, a secondary minimum in free energy appears for $\alpha \neq 0$, corresponding to a thermodynamically stable ordered nematic phase. This may not immediately indicate an equilibrium state; indeed Onsager recognised that the free energy may be lowered further by macroscopic phase separation (although we do not expect to observe this in the system sizes considered here).

Numerical calculation gives ν^*, from which the critical volume fraction ϕ^* may be obtained for rigid rods:

$$\nu^* = \frac{16}{\pi DL^2}, \qquad \phi^* = \nu^* \frac{\pi D^2 L}{4} \simeq 4\frac{D}{L} \qquad (12)$$

To derive (9) that we have assumed it is valid to ignore the third (and higher) Virial coefficients. The reduced third virial coefficient scales as $(D/L)\log(L/D)$, and so is relatively small for the systems considered here. While it should be remembered this may introduce some error in the absolute volume fraction for the phase transition, it does not affect the validity of the phases observed themselves.

Despite its importance in simulation, ~~it~~ tt is also acknowledged that this is a typically poor model experimentally; primarily because physical systems either have much lower aspect ratios or are not truly rigid [**Odijk1985**]. In this case, the long-range Maier–Snape theory [**Maier1959**] is typically used, with the additional benefit that this also accounts for attractive inter-molecular forces. This produces significantly more accurate estimates of the critical volume fraction and the order parameter at the isotropic–nematic transition [**Zannoni1979b**].

Appendix B   Nematic Order Parameter

B.1   Theoretical Outline

Here I endeavour to outline the motivation for the nematic order parameter used throughout this report, based on the work of Eppenga and Frenkel [**Eppenga1984**, **Frenkel1982**]. The nematic phase may be differentiated from the isotropic phase by the formation of cylindrical symmetry, as opposed to the spherical symmetry of the isotropic phase. The deviation from spherical symmetry may be quantified through a set of order parameters [**Zannoni1979**]. When considering the axially symmetric nematic phase, independent of ϕ, the distribution function $f(\theta, \phi)$ may be generally expressed in the basis of all even Legendre polynomials P_{2l}:

$$f(\theta) = \sum_{l=0}^{\infty} a_{2l} P_{2l}(\cos(\theta)) \tag{13}$$

where θ is the angle between the molecular orientation and the axis of symmetry of the system. Note that odd-ordered terms are neglected for nonpolar molecules, as the director may point in either of two antiparallel directions and so all odd Legendre polynomials average to zero [**Parsons1979**].

In an isotropic phase, a_{2l} vanishes for all $l > 0$, so all angular dependence vanishes. More generally, quantities $\langle P_{2l}(\cos(\theta)) \rangle$ may be used at the order parameter of the system, with the second order term being referred to as the nematic order parameter. Averaging over a population of N molecules, we can therefore write the nematic order parameter S_n as:

$$S_n = \frac{1}{N} \left\langle \sum_{i=1}^{N} \left(\frac{3}{2} \cos^2(\theta_i) - \frac{1}{2} \right) \right\rangle \tag{14}$$

B.2   Calculation

The method given above in Appendix B.1 relies on knowledge of the system-wide nematic director (ie the axis of symmetry of the cylindrical phase), to define θ_i. However, this is not always possible in physical systems where such a unique direction is not externally imposed.

Instead, as detailed by Frenkel et al. [**Frenkel1985**], we maximise the expression:

$$S_n'(\hat{\boldsymbol{n}}') = \frac{1}{N} \left[\sum_{i=1}^{N} \left(\frac{3}{2} (\hat{\boldsymbol{n}}' \cdot \hat{\boldsymbol{u}}_i)^2 - \frac{1}{2} \right) \right] \tag{15}$$

where $\hat{u}_i$ denotes the orientation of the individual molecular axes in the laboratory frame, and $(\hat{\boldsymbol{n}}')$ is the direction of common alignment, known as the director. In the absence of an electric field, the direction of this is arbitrary, and determined in practice by infinitesimal perturbations to the system though spontaneous symmetry breaking [**Forster2018**]. (15) may be further simplified to:

$$S_n' = \frac{1}{N} \left\langle \hat{\boldsymbol{n}}' \cdot \mathbf{Q} \cdot \hat{\boldsymbol{n}}' \right\rangle, \qquad where \ \mathbf{Q}_i = \frac{3}{2} \hat{\boldsymbol{u}}_i \hat{\boldsymbol{u}}_i - \frac{1}{2} \mathbf{I} \tag{16}$$

The tensor order parameter $\langle \mathbf{Q} \rangle$ is a traceless symmetric 2nd-rank tensor, with three eigenvalues $\lambda_+, \lambda_0, \lambda_-$ [**Eppenga1984**]. We typically take the largest eigenvalue (λ_+) as the nematic order parameter, a good approximation in large N limit. In practice, we actually calculate the eigenvalues of the related tensor $\mathbf{M}$:

$$\mathbf{M} = \frac{1}{N} \sum_{i=1}^{N} \hat{\boldsymbol{u}}_i \hat{\boldsymbol{u}}_j \tag{17}$$

as this shares eigenvectors with $\mathbf{Q}$, and has eigenvectors μ_n related to λ_n by: $\mu_n = 2/3\lambda_n + 1/3$.

It is worth noting λ_+ is bound above zero, and so does not reach zero in the isotropic phase as would be expected. It is common to use $S = -2\lambda_0$ when considering such disordered systems, as this fluctuates about an average much closer to zero [**Mountain1977**]. I have not done so in the results presented here, to give continuity in the order parameter over the transition (wherein lies the focus of this report), however this has meant that the average order parameter in the isotropic phase is slightly above zero.

B.3   Position Dependant Order Parameter

The pairwise orientational correlation function, introduced in Section 5.3 and given in equation (4), provides an equivalent to the nematic order parameter that is position dependant. For use in simulation, we rewrite this for N particles in the form:

$$g_l(r) = \frac{\sum_{i=1}^{N} \sum_{j \neq i} P_l(\hat{\boldsymbol{u}_i} \cdot \hat{\boldsymbol{u}_j}) \Delta(r_{ij} - r)}{\sum_{i=1}^{N} \sum_{j \neq i} \Delta(r_{ij} - r)} \tag{18}$$

where $\Delta(r_{ij} - r) = 1$ if r_{ij} is inside a spherical shell between r and $r + \delta$, and 0 otherwise. The thickness of δ is chosen to maximise the resolution of the function, as too large a value will 'wash out' important features, while still maintaining a reasonable sample size. This method is very computationally expensive however, as the number of times P_L must be calculated scales as $\mathcal{O}(N^2)$. Furthermore, the storage of all necessary angles is prohibitively expensive (even on modern computers), and limits the resolution possible here [**Soper1998**]. We may however avoid this problem by expanding the function in terms of spherical harmonics, and sum the contributions for all pairs to a given molecule [**Soper1994**]. This is most easily done through application of the spherical harmonics addition theorem:

$$P_l(\cos\theta_{ij}) = \frac{4\pi}{2l+1} \sum_{m=-l}^{l} \mathcal{Y}_{lm}(\hat{\boldsymbol{u}_i}) \mathcal{Y}_{lm}^*(\hat{\boldsymbol{u}_j}) \tag{19}$$

Using this, recognising that $\hat{\boldsymbol{u}_i} \cdot \hat{\boldsymbol{u}_j} = \cos\theta_{ij}$ and writing $\Delta(r_{ij} - r) = \Delta_r$ for simplicity, we may write the contribution from all particles around particle i as:

$$\sum_{i \neq j} P_l(\cos\theta_{ij}) \Delta_r = \frac{4\pi}{2l+1} \sum_{j \neq i} \sum_{m=-l}^{l} \mathcal{Y}_{lm}(\hat{\boldsymbol{u}_i}) \mathcal{Y}_{lm}^*(\hat{\boldsymbol{u}_j}) \Delta_r \tag{20}$$

Exchanging the order of summation, and removing $\mathcal{Y}_{lm}(\hat{\boldsymbol{u}_i})$ from the sum over j gives:

$$\sum_{i \neq j} P_l(\cos\theta_{ij}) \Delta_r = \frac{4\pi}{2l+1} \sum_{m=-l}^{l} \mathcal{Y}_{lm}(\hat{\boldsymbol{u}_i}) \sum_{j \neq i} \mathcal{Y}_{lm}^*(\hat{\boldsymbol{u}_j}) \Delta_r \tag{21}$$

This may be simplified further to:

$$\sum_{i \neq j} P_l(\cos\theta_{ij}) \Delta_r = \frac{4\pi}{2l+1} \sum_{m=-l}^{l} \mathcal{Y}_{lm}(\hat{\boldsymbol{u}_i}) \times C_{lm}^* \tag{22}$$

where we have defined

$$C_{lm}^* = \sum_{j \neq i} \mathcal{Y}_{lm}^*(\hat{\boldsymbol{u}_j}) \Delta_r \tag{23}$$

This removes the requirement to calculate P_l for every pair of molecules, in favour of simply summing the spherical harmonics terms corresponding to a given shell around i, then multiply spherical harmonics components. It should also be noted that (22) is invariant under changes in the coordinate frame; in our computations all orientations were expressed in the lab frame for each (rather than aligning the coordinate frame with the global director).

Appendix C   Mean Squared Displacement

Here, we provide a derivation of the diffusion relation (6), taking a popular approach through the derivation of the moment generating function [**Mazo2008**, **Gardiner2009**]. The diffusive motion of a particle is a stochastic process, which may be described by a probability density function (PDF) that satisfies the diffusion equation:

$$\frac{\partial p(x, t \mid x_0)}{\partial t} = D \frac{\partial^2 p(x, t \mid x_0)}{\partial x^2} \tag{24}$$

where $x(t)$ is the position of the particle at some time t, and x_0 is the initial position of the particle. For simplicity we will use a one dimensional space here, but the argument is easily extended to higher dimensions.

This is trivially obeyed by the Green's function $G(x, t)$, where this is defined to be the time evolution of density $G(x, 0) = \delta(x)$ (taking $x_0 = 0$ for simplicity). We must therefore first obtain $G(x, t)$ for which we will use Fourier transform methods based on the approach by Sethna [**Sethna2006**]. In general, we may decompose our solution into a family of plane wave solutions of the form $\tilde{p}_k(t)e^{ikx}$. Substituting this into (24), we obtain

$$\frac{\partial p}{\partial t} = \frac{d\tilde{p}_k}{dt} e^{ikx} = D \frac{\partial^2 p}{\partial x^2} = -Dk^2 \tilde{p}_k(t) e^{ikx} \tag{25}$$

from which we may extract a differential equation in $\tilde{p}_k(t)$, with the simple solution:

$$\tilde{p}_k(t) = \tilde{p}_k(0) e^{-Dk^2 t} \tag{26}$$

The Fourier transform of $G(x, t)$ at $t = 0$ is given by:

$$\tilde{G}_k(0) = \int G(x, 0) e^{-ikx} dx = \int \delta(x) e^{-ikx} dx = 1 \tag{27}$$

and so the time dependant Fourier transform is given by $\tilde{G}_k(t) = e^{-Dk^2 t}$ according to (26). This gives a the real-space $G(x, t)$ as:

$$G(x, t) = \frac{1}{2\pi} \int e^{ikx} \tilde{G}_k(0) e^{-Dk^2 t} dk = \frac{1}{2\pi} \int e^{ikx} e^{-Dt^k t} dk \tag{28}$$

This is simply the inverse Fourier transform of a Gaussian, and so evaluates to:

$$G(x, t) = \frac{1}{\sqrt{4\pi D t}} e^{-x^2/4Dt} \tag{29}$$

Redefining the spatial coordinate to account for the initial conditions, the probablility density function is given by:

$$P(x, t) = \frac{1}{\sqrt{4\pi D t}} e^{-(x-x_0)^2/4Dt} \tag{30}$$

Using this function, the average of an arbitrary function A at time t is given by:

$$\langle A(t) \rangle = \int_{-\infty}^{\infty} A(x, t) P(x, t) dx \tag{31}$$

This must be evaluated for the mean squared displacement (MSD):

$$\langle (x(t) - x_0)^2 \rangle = \langle x^2 \rangle + x_0^2 - 2x_0 \langle x \rangle \tag{32}$$

While it is possible to evaluate $\langle x \rangle$ and $\langle x^2 \rangle$ explicitly, it is perhaps more elegant to find the moment generating function, which describes the k-th moment of the PDF. We first introduce the characteristic function:

$$\phi_x(k) = \langle e^{ikx} \rangle = \int e^{ikx} P(x, t \mid x_0) dx = \sum_{n=0}^{\infty} \frac{(ik)^n}{n!} \langle x^n \rangle \tag{33}$$

where $\langle x^n \rangle$ are the moments of $P(x)$. We may separately define the cumulants C_n by writing $\phi_x(k)$ in the form (the motivation for which will shortly be apparent):

$$\phi_x(k) = \exp\left[\sum_{n=0}^{\infty} \frac{(ik)^n}{n!} C_n \right] \tag{34}$$

Comparing coefficients with (33), we may identify the cumulants explicitly as:

$$C_n = \frac{d^n}{d(ik)^n} \ln\left(\phi_x(k)\right) \Big|_{k=0} \tag{35}$$

As (33) may be evaluated by completing the square to give the form:

$$\phi_x(k) = e^{ikx_0 - k^2 Dt} \tag{36}$$

we find by simple substitution that the first two cumulants are given by:

$$C_1 = x_0, \qquad C_2 = 2Dt \tag{37}$$

Note that this value for C_1 is expected, as it corresponds to the mean of the Gaussian distribution. Substitution of these values into (32) renders the desired result:

$$\langle (x(t) - x_0)^2 \rangle = 2Dt \tag{38}$$